Comparative analysis of the fusion reactions ^{48}Ti + ^{58}Fe and ^{58}Ni + ^{54}Fe

V. V. Sargsyan,[1] G. G. Adamian,[1] N. V. Antonenko,[1,2] W. Scheid,[3] and H. Q. Zhang[4]
[1]*Joint Institute for Nuclear Research, 141980 Dubna, Russia*
[2]*Mathematical Physics Department, Tomsk Polytechnic University, 634050 Tomsk, Russia*
[3]*Institut für Theoretische Physik der Justus-Liebig-Universität, D-35392 Giessen, Germany*
[4]*China Institute of Atomic Energy, Post Office Box 275, Beijing 102413, China*
(Received 15 January 2017; published 30 May 2017)

The experimental fusion excitation functions of the reactions ^{48}Ti + ^{58}Fe and ^{58}Ni + ^{54}Fe, measured down to the low sub-barrier energies, are described within the quantum diffusion approach and the universal fusion function representation. For these systems, the s-wave capture probabilities are extracted from the experimental excitation functions and are also analyzed. An enhancement of the sub-barrier fusion cross section observed in the ^{48}Ti + ^{58}Fe reaction in comparison to the relatively close system ^{58}Ni + ^{54}Fe is explained.

DOI: 10.1103/PhysRevC.95.054619

I. INTRODUCTION

Heavy-ion fusion near and below the Coulomb barrier is attracting experimental and theoretical interest [1,2]. This study is particularly important for the synthesis of superheavy elements at near barrier energies [3–5] and for the astrophysical reactions at sub-barrier energies [1,2]. The nature of the fusion hindrance phenomenon in the reactions with various medium-light and heavy nuclei, where at deep sub-barrier energies the fusion cross sections drop faster than coupled-channels calculations, is not yet completely understood [2,6]. An experimental study of the ^{48}Ti + ^{58}Fe reaction at sub-barrier energies, at which no data existed previously, and a comparison with relatively close system ^{58}Ni + ^{54}Fe have been recently performed in Ref. [7]. The difference of the two systems in nuclear structure is notable. Indeed, ^{48}Ti + ^{58}Fe are soft and have the low-lying quadrupole excitation states. Instead, ^{58}Ni + ^{54}Fe are closed-shell nuclei and are rather rigid. The octupole vibrational states are high in energy and hardly excited, in all cases. As observed, the fusion cross sections in the ^{58}Ni + ^{54}Fe reaction decrease very steeply toward the lowest energies. The coupled-channels calculations performed with CCFULL [7] reproduce the experimental data for the ^{48}Ti + ^{58}Fe reaction, but strongly overestimate the cross sections below $\simeq$200 μb for the ^{54}Fe + ^{58}Ni reaction. So, the fusion hindrance effects show up already at the level of relatively large cross sections [8]. Note that in the ^{48}Ti + ^{58}Fe reaction, the two-neutron transfer channel with a positive Q_{2n} value ($Q_{2n} = 1.4$ MeV) has been ignored.

Applying the quantum diffusion approach [9–13] (Sec. IV), the universal fusion function representation [14–16] (Sec. II), and capture probabilities extracted from the experimental excitation functions (Sec. III), we try to answer the question how the quadrupole deformation effect influences the sub-barrier capture cross section in the reactions ^{48}Ti + ^{58}Fe and ^{58}Ni + ^{54}Fe at near and sub-barrier energies. We will show why the influence of positive Q_{2n}-value neutron transfer does not play a role in the ^{48}Ti + ^{58}Fe reaction. For these reactions, the S and L factors, and the barrier distributions will be also discussed. The S-factor and L-factor representations of the measured cross sections have been introduced in Ref. [6] to show the fusion hindrance effect without invoking model calculations.

II. EXPERIMENTAL REDUCED FUSION (CAPTURE) CROSS SECTIONS

To analyze the fusion cross sections $\sigma_f(E_{\rm c.m.})$ in the reactions with different Coulomb barrier heights V_b and radii R_b calculated in the case of spherical nuclei, it is useful to compare the dimensionless quantities

$$\sigma_f \rightarrow F(x) = 2E_{\rm c.m.}\sigma_f(E_{\rm c.m.})/\left(\hbar\omega_b R_b^2\right)$$

versus

$$E_{\rm c.m.} \rightarrow x = (E_{\rm c.m.} - V_b)/(\hbar\omega_b)$$

[14–16] instead of the excitation functions. Here, ω_b and μ are the frequency of an inverted oscillator approximated the barrier and the reduced mass of the system, respectively. In this way the geometrical and barrier hight effects can be eliminated. This reduction method is suggested by Wong's formula

$$\sigma_f(E_{\rm c.m.}) = \frac{\hbar\omega_b R_b^2}{2E_{\rm c.m.}} \ln[1 + \exp(2\pi[E_{\rm c.m.} - V_b]/(\hbar\omega_b))]$$

for the fusion cross section [17]. This analytic expression is derived by approximating the barrier by an inverse parabola and neglecting the variation of the barrier radius with angular momentum. In this case

$$F(x) \rightarrow F_0(x) = \ln[1 + \exp(2\pi x)].$$

It is the same function for any fusion reaction. For this reason, it is called the universal fusion function (UFF).

In the reactions, where the capture and fusion cross sections coincide [$\sigma_f(E_{\rm c.m.}) = \sigma_{\rm cap}(E_{\rm c.m.})$], the comparison of experimental data with the universal fusion function [14–16] allows us to conclude about the role of static deformations of the colliding nuclei and the nucleon transfer between them in the capture cross section. Indeed, the universal function disregards these effects. To obtain the values of V_b, R_b, and ω_b, we calculate the nucleus-nucleus interaction potential. The same potential is used within the quantum diffusion approach

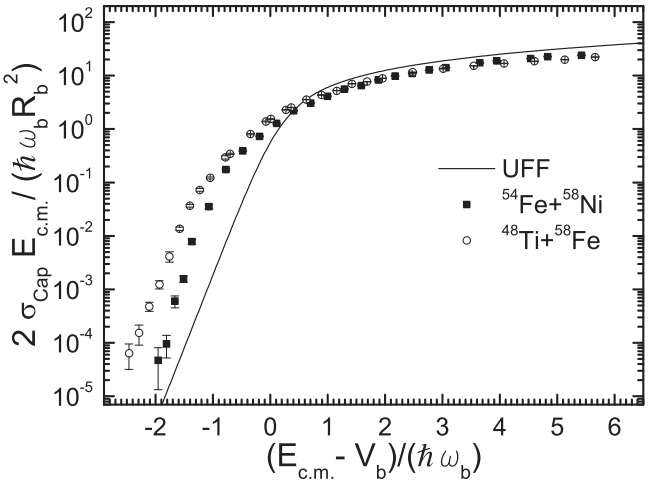

FIG. 1. The experimental reduced fusion excitation functions $\frac{2E_{\rm c.m.}}{\hbar\omega_b R_b^2}\sigma_{\rm cap}(E_{\rm c.m.})$ [7,8] (symbols) and the universal fusion function $F_0 = \ln(1+\exp[2\pi(E_{\rm c.m.}-V_b)/(\hbar\omega_b)])$ (solid line) vs $\frac{E_{\rm c.m.}-V_b}{\hbar\omega_b}$ for the reactions indicated. The experimental data have uncertainty bars because of the uncertainties of experimental $\sigma_{\rm cap}(E_{\rm c.m.})$ and $E_{\rm c.m.}$.

[9–13] (see Sec. IV). The $V_b = 91.8$ MeV, $\hbar\omega_b = 3.3$ MeV, $R_b = 11.02$ fm and $V_b = 72.3$ MeV, $\hbar\omega_b = 3.1$ MeV, $R_b = 11.08$ fm are obtained for the ^{54}Fe + ^{58}Ni and ^{48}Ti + ^{58}Fe systems, respectively. The experimental data have uncertainty bars because of the uncertainties of experimental $\sigma_{\rm cap}(E_{\rm c.m.})$ and $E_{\rm c.m.}$. The experimental uncertainties are evaluated in the following way. At given average $E_{\rm c.m.}[\sigma_{\rm cap}(E_{\rm c.m.})]$, we perform the calculations with the maximum, minimum, and average $\sigma_{\rm cap}(E_{\rm c.m.})[E_{\rm c.m.}]$ (Fig. 1).

For the ^{54}Fe + ^{58}Ni reaction with almost spherical nuclei and without neutron transfer (the negative Q_{xn} values), the experimental cross sections are more closer to the universal fusion function (Fig. 1). For the ^{48}Ti + ^{58}Fe reaction with soft nuclei and with the two-neutron transfer (the positive Q_{2n} value), one can clearly see that the reduced cross sections strongly deviate from those for the ^{54}Fe + ^{58}Ni reaction and from the universal fusion function (Fig. 1). So, the experimental reduced excitation function of the ^{48}Ti + ^{58}Fe reaction shows a large enhancement with respect to the ^{54}Fe + ^{58}Ni reaction at sub-barrier energies. This difference of the experimental reduced excitation functions is probably caused by the deformation or/and the neutron transfer effects.

III. CAPTURE PROBABILITIES EXTRACTED FROM THE EXPERIMENTAL CROSS SECTIONS

Shifting the energy by the rotational energy $E_R(J) = \frac{\hbar^2 J(J+1)}{2\mu R_b^2}$ [18], one can approximate the angular momentum J dependence of the transmission (capture) probability $P_{\rm cap}(E_{\rm c.m.}, J)$, at a given $E_{\rm c.m.}$:

$$P_{\rm cap}(E_{\rm c.m.}, J) \approx P_{\rm cap}(E_{\rm c.m.} - E_R(J), J = 0). \quad (1)$$

If we use the formula for the capture cross section, convert the sum over the partial waves J into an integral, and express J via the variable $E = E_{\rm c.m.} - E_R(J)$, we obtain the following simple expression:

$$\sigma_{\rm cap}(E_{\rm c.m.}) = \frac{\pi R_b^2}{E_{\rm c.m.}} \int_0^{E_{\rm c.m.}} dE\, P_{\rm cap}(E, J = 0). \quad (2)$$

Multiplying this equation by $E_{\rm c.m.}/(\pi R_b^2)$ and differentiating over $E_{\rm c.m.}$, one obtains [18]

$$P_{\rm cap}(E_{\rm c.m.}, J = 0) = \frac{1}{\pi R_b^2} \frac{d[E_{\rm c.m.}\sigma_{\rm cap}(E_{\rm c.m.})]}{dE_{\rm c.m.}}. \quad (3)$$

One can see that $\frac{d[E_{\rm c.m.}\sigma_{\rm cap}(E_{\rm c.m.})]}{dE_{\rm c.m.}}$ has a meaning of the s-wave transmission in the entrance channel. Therefore, the s-wave capture probability can be extracted with a satisfactory accuracy from the experimental capture cross sections $\sigma_{\rm cap}(E_{\rm c.m.})$ at energies near and below the Coulomb barrier. Note that at energies considered the dependence of the Coulomb barrier radius on the angular momentum is very weak.

The experimental s-wave capture probabilities are extracted with a two-point difference formula:

$$P_{\rm cap}(E_{\rm c.m.}, J = 0) \approx \frac{1}{\pi R_b^2} \frac{\left(E_{\rm c.m.} + \frac{\Delta E_{\rm c.m.}}{2}\right)\sigma_{\rm cap}\left(E_{\rm c.m.} + \frac{\Delta E_{\rm c.m.}}{2}\right) - \left(E_{\rm c.m.} - \frac{\Delta E_{\rm c.m.}}{2}\right)\sigma_{\rm cap}\left(E_{\rm c.m.} - \frac{\Delta E_{\rm c.m.}}{2}\right)}{\Delta E_{\rm c.m.}}.$$

The $P_{\rm cap}(E_{\rm c.m.}, J = 0)$ is obtained as the incremental ratio for successive pairs of experimental energy points of the of the excitation function. At deep sub-barrier energies the difference between the experimental points about 0.5 MeV. The experimental uncertainties are evaluated in the same way as for the UFF. In Figs. 2 and 3, the extracted capture probabilities $P_{\rm cap}(E, J = 0)$ demonstrate the influence of the deformation or/and the neutron transfer effects on the capture (fusion) excitation function. In the ^{54}Fe + ^{58}Ni reaction with the closed shell nuclei and with the negative Q_{2n} values for neutron transfer, the capture probability exhibits a steep falloff at low energies. Conversely, in the ^{48}Ti + ^{58}Fe reaction with the soft nuclei and with the positive Q_{2n} value for neutron transfer, the capture probability has a smaller slope at sub-barrier energies (Fig. 3).

As follows from the extracted s-wave capture probabilities (Figs. 2 and 3), $P_{\rm cap}(^{58}{\rm Ni} + ^{54}{\rm Fe}) \approx P_{\rm cap}(^{48}{\rm Ti} + ^{58}{\rm Fe})$ at energies from $E_{\rm c.m.} - V_b \approx 0$ MeV to $E_{\rm c.m.} - V_b \approx 8$ MeV and there are discrepancies between $P_{\rm cap}(^{58}{\rm Ni} + ^{54}{\rm Fe})$ and $P_{\rm cap}(^{48}{\rm Ti} + ^{58}{\rm Fe})$ at energies $E_{\rm c.m.} - V_b > 8$ MeV. Firstly the extracted $P_{\rm cap}$ increases with $E_{\rm c.m.}$ above the Coulomb barrier and after it starts to decrease. One should think about the experimental reasons for such deviations and behavior.

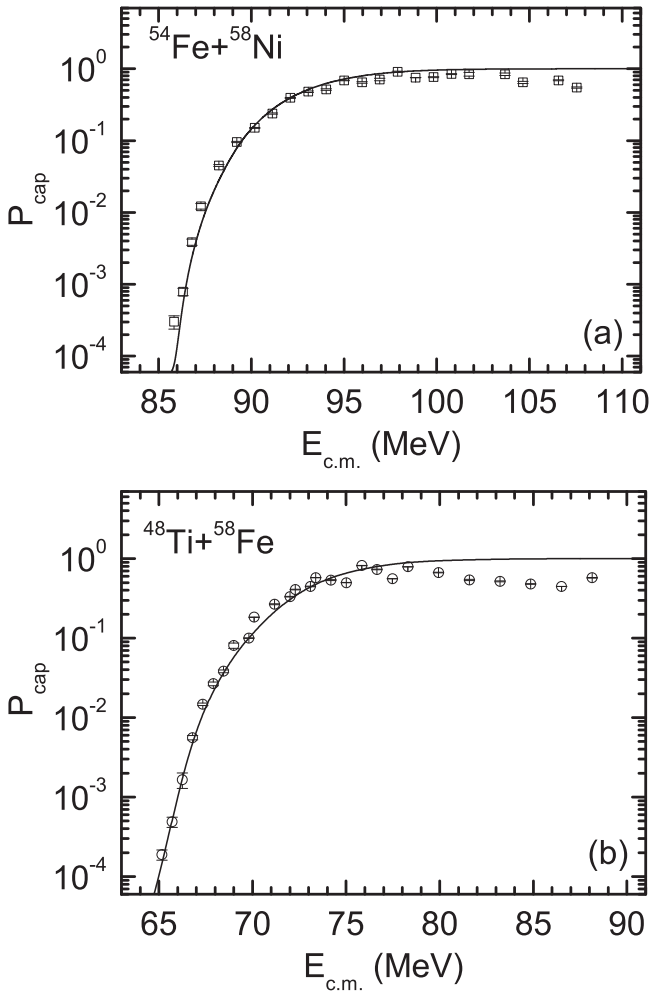

FIG. 2. The extracted (symbols) and calculated (lines) s-wave capture probabilities versus $E_{\mathrm{c.m.}}$ for the reactions indicated. The experimental P_{cap} is obtained as the incremental ratio for the successive pairs of experimental points. The used experimental capture (fusion) excitation functions are from Refs. [7,8]. The experimental data have uncertainty bars because of the uncertainties of experimental $\sigma_{\mathrm{cap}}(E_{\mathrm{c.m.}})$ and $E_{\mathrm{c.m.}}$.

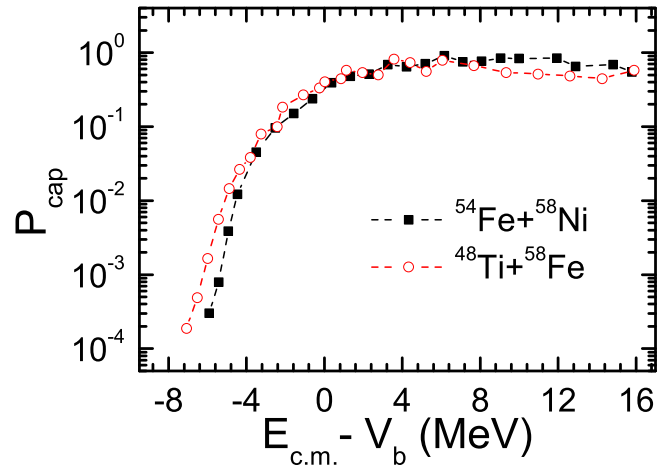

FIG. 3. The extracted (symbols connected by lines) s-wave capture probabilities versus $E_{\mathrm{c.m.}} - V_b$ for the reactions indicated. The experimental P_{cap} is obtained as the incremental ratio for the successive pairs of experimental points. The used experimental capture (fusion) excitation functions are from Refs. [7,8].

IV. CALCULATIONS WITHIN THE QUANTUM DIFFUSION APPROACH

A. Model

In the quantum diffusion approach [9–13] the collisions of nuclei are described with the single relevant collective variable: the relative distance between the colliding nuclei. This approach takes into consideration the fluctuation and dissipation effects in collisions of heavy ions which model the coupling with various channels (for example, the noncollective single-particle excitations, low-lying collective dynamical modes of the target and projectile). We have to mention that many quantum-mechanical and non-Markovian effects accompanying the passage through the potential barrier are taken into consideration in our formalism [9–13]. The nuclear deformation effects are taken into account through the dependence of the nucleus-nucleus potential on the deformations and mutual orientations of the colliding nuclei. With this approach many heavy-ion capture reactions at energies above and well below the Coulomb barrier have been successfully described [9–13].

The capture cross section is a sum of partial capture cross sections [9,10]

$$\sigma_{\mathrm{cap}}(E_{\mathrm{c.m.}}) = \sum_J \sigma_{\mathrm{cap}}(E_{\mathrm{c.m.}},J) = \pi\lambda\!\!\!^{-2} \sum_J (2J+1) \int_0^{\pi/2} d\theta_1 \sin(\theta_1) \int_0^{\pi/2} d\theta_2 \times \sin(\theta_2) P_{\mathrm{cap}}(E_{\mathrm{c.m.}},J,\theta_1,\theta_2), \quad (4)$$

where $\lambda\!\!\!^{-2} = \hbar^2/(2\mu E_{\mathrm{c.m.}})$ is the reduced de Broglie wavelength, $\mu = m_0 A_1 A_2/(A_1+A_2)$ is the reduced mass (m_0 is the nucleon mass), and the summation is over the possible values of angular momentum J at a given bombarding energy $E_{\mathrm{c.m.}}$. Knowing the potential of the interacting nuclei for each orientation, one can obtain the partial capture probability P_{cap} which is defined by the passing probability of the potential barrier in the relative distance R coordinate at a given J. The value of P_{cap} is obtained by integrating the propagator G from the initial state (R_0,P_0) at time $t=0$ to the final state (R,P) at time t (P is a momentum):

$$P_{\mathrm{cap}} = \lim_{t\to\infty} \int_{-\infty}^{r_{\mathrm{in}}} dR \int_{-\infty}^{\infty} dP\; G(R,P,t|R_0,P_0,0) = \lim_{t\to\infty} \frac{1}{2}\mathrm{erfc}\left[\frac{-r_{\mathrm{in}}+\overline{R(t)}}{\sqrt{\Sigma_{RR}(t)}}\right]. \quad (5)$$

The second line in Eq. (5) is obtained by using the propagator $G = \pi^{-1}|\det\Sigma^{-1}|^{1/2}\exp(-\overline{\mathbf{q}^T\Sigma^{-1}\boldsymbol{q}})$ $[\mathbf{q}^T = [q_R,q_P]$, $q_R(t) = R - \overline{R(t)}$, $q_P(t) = P - \overline{P(t)}$, $\overline{R(t=0)} = R_0$, $\overline{P(t=0)} = P_0$, $\Sigma_{kk'}(t) = 2\overline{q_k(t)q_{k'}(t)}$, $\Sigma_{kk'}(t=0) = 0$, $k,k' = R,P]$ calculated calculated in Ref. [19] for the inverted oscillator, which approximates the nucleus-nucleus interaction

potential V (nuclear + Coulomb + centrifugal potentials) in the variable R and has the frequency $\omega = \omega(E_{\rm c.m.})$ depending on the bombarding energy $E_{\rm c.m.}$ and internal turning point $r_{\rm in}$. At each sub-barrier energy $E_{\rm c.m.}$, the value of ω is defined from the condition of equality of the classical actions of the approximated and realistic potential barriers of the same height at given J. At bombarding energies above the Coulomb barrier $V(R_b)$ at the position $R = R_b$, $\omega = (|\partial^2 V/\partial R^2|_{R=R_b}/\mu)^{1/2}$. As found at $E_{\rm c.m.} > V(R_b)$, the capture cross section weakly depends on ω. This approximation is well justified for the reactions and energy range, which are here considered [9–13]. Finally, one can find the expression for the capture probability

$$P_{\rm cap} = \frac{1}{2}{\rm erfc}\left[\left(\frac{\pi s_1(\gamma - s_1)}{2\hbar\mu\left(\omega_0^2 - s_1^2\right)}\right)^{1/2}\frac{\mu\omega_0^2 R_0/s_1 + P_0}{[\gamma\ln(\gamma/s_1)]^{1/2}}\right], \quad (6)$$

where γ is the internal-excitation width, $\omega_0^2 = \omega^2\{1 - \hbar\tilde{\lambda}\gamma/[\mu(s_1+\gamma)(s_2+\gamma)]\}$ is the renormalized frequency in the Markovian limit, the value of $\tilde{\lambda}$ is related to the strength of linear coupling in coordinates between collective and internal subsystems. The s_i are the real roots ($s_1 \geqslant 0 > s_2 \geqslant s_3$) of the following equation:

$$(s+\gamma)\left(s^2 - \omega_0^2\right) + \hbar\tilde{\lambda}\gamma s/\mu = 0. \quad (7)$$

The details of the used formalism are presented in [9,10]. We have to mention that most of the quantum-mechanical, dissipative effects and non-Markovian effects accompanying the passage through the potential barrier are taken into consideration in our formalism [9,10]. For example, the non-Markovian effects appear in the calculations through the internal-excitation width γ.

As shown in [9,10], the nuclear forces start to play a role at $R_{\rm int} = R_b + 1.1$ fm where the nucleon density of colliding nuclei approximately reaches 10% of the saturation density. If the value of $r_{\rm ex}$ corresponding to the external turning point is larger than the interaction radius $R_{\rm int}$, we take $R_0 = r_{\rm ex}$ and $P_0 = 0$ in Eq. (6). For $r_{\rm ex} < R_{\rm int}$, it is naturally to start our treatment with $R_0 = R_{\rm int}$ and P_0 defined by the kinetic energy at $R = R_0$. In this case the friction hinders the classical motion to proceed towards smaller values of R. If $P_0 = 0$ at $R_0 > R_{\rm int}$, the friction almost does not play a role in the transition through the barrier. Thus, two regimes of interaction at sub-barrier energies differ by the action of the nuclear forces and the role of friction at $R = r_{\rm ex}$.

Besides the parameters related to the nucleus-nucleus potential, two parameters $\hbar\gamma = 15$ MeV and the friction coefficient $\hbar\lambda = -\hbar(s_1 + s_2) = 2$ MeV are used for calculating the capture probability in reactions with deformed actinides. The value of $\tilde{\lambda}$ is set to obtain this value of $\hbar\lambda$. The most realistic friction coefficients in the range of $\hbar\lambda \approx 1$–2 MeV are suggested from the study of deep inelastic and fusion reactions [20]. These values are close to those calculated within the mean field approach [21]. All calculated results presented are obtained with the same set of parameters and are rather insensitive to a reasonable variation of them [9,10]. All parameters of the model are set as in Ref. [9]. All calculated results are obtained with the same set of parameters and are rather insensitive to the reasonable variation of them [9,10]. To calculate the nucleus-nucleus interaction potential $V(R)$, we use the procedure presented in Refs. [9–13]. For the nuclear part of the nucleus-nucleus potential, the double-folding formalism with the Skyrme-type density-dependent effective nucleon-nucleon interaction is used. The parameters of the nucleus-nucleus interaction potential $V(R)$ are adjusted to describe the experimental data at energies near the Coulomb barrier [$V_b = V(R_b)$] corresponding to spherical nuclei.

Following the hypothesis of Ref. [22], we assume that the sub-barrier capture in the reactions under consideration mainly depends on the two-neutron transfer with the positive Q_{2n} value. Our assumption is that, before the projectile is captured by the target-nucleus (just before the crossing of the Coulomb barrier), which is a slow process, the $2n$ transfer ($Q_{2n} > 0$) occurs and leads to the population of the first excited collective state in the recipient nucleus at $Q_{2n} \geqslant E_{2^+}$ or of the ground state in the recipient nucleus at $Q_{2n} < E_{2^+}$ [23]. Here, E_{2^+} is the energy of the first excited 2^+ state. The donor nucleus remains in the ground state. The absolute values of the quadrupole deformation parameters β_2 in the first 2^+ state of even-even deformed nuclei are taken from Ref. [24]. For the nuclei deformed in the ground state, the β_2 in the first excited collective state is similar to that in the ground state. For instance, $\beta_2(^{56}{\rm Fe}) = 0.24$ and $\beta_2(^{58}{\rm Fe}) = 0.26$ [24]. For the double magic and semimagic nuclei, we take $\beta_2 = 0$ or 0.05 in the ground state. For example, $\beta_2(^{58}{\rm Ni}) = 0.05$ [10] and $\beta_2(^{50}{\rm Ti}) = \beta_2(^{54}{\rm Fe}) = 0$.

The motion to N/Z equilibrium starts in the system before the capture occurs because it is energetically favorable in the dinuclear system in the vicinity of the Coulomb barrier. For the reactions under consideration, the average change of mass asymmetry is related to the two-neutron transfer. In these reactions, $Q_{2n} > Q_{1n}$ and during the capture the $2n$ transfer is more probable than $1n$ transfer. After the $2n$ transfer the mass numbers, the deformation parameters of the interacting nuclei, and, correspondingly, the height V_b and shape of the Coulomb barrier change. Then one can expect an enhancement or suppression of the capture. If after the neutron transfer the deformations of interacting nuclei increase (decrease), the capture probability increases (decreases). If after the transfer the deformations of interacting nuclei do not change, there is no effect of the neutron transfer on the capture. This scenario was verified in the description of many reactions [9–13].

B. Capture probabilities and cross sections

In Figs. 2 and 4, one can see a good agreement between the calculated and the experimental capture probabilities and cross sections in the $^{48}{\rm Ti} + {}^{58}{\rm Fe}$ reaction (lower part) with the positive Q values for neutron transfer and in the $^{58}{\rm Ni} + {}^{54}{\rm Fe}$ reaction (upper part) with negative Q values for neutron transfer. The theoretical calculations describe the strong deviation of the slopes of excitation functions in the reactions $^{58}{\rm Ni} + {}^{54}{\rm Fe}$ and $^{48}{\rm Ti} + {}^{58}{\rm Fe}$ at sub-barrier energies. However, the observed capture enhancement in the $^{48}{\rm Ti} + {}^{58}{\rm Fe}$ reaction is not related to the two-neutron transfer effect. After $2n$ transfer ($0 < Q_{2n} < E_{2^+} = 1.55$ MeV) in this reaction [before capture (fusion)] $^{48}{\rm Ti} + {}^{58}{\rm Fe} \rightarrow {}^{50}{\rm Ti} + {}^{56}{\rm Fe}$ the deformations of nuclei decrease because they approach the closed shells and the height of the Coulomb barrier increases.

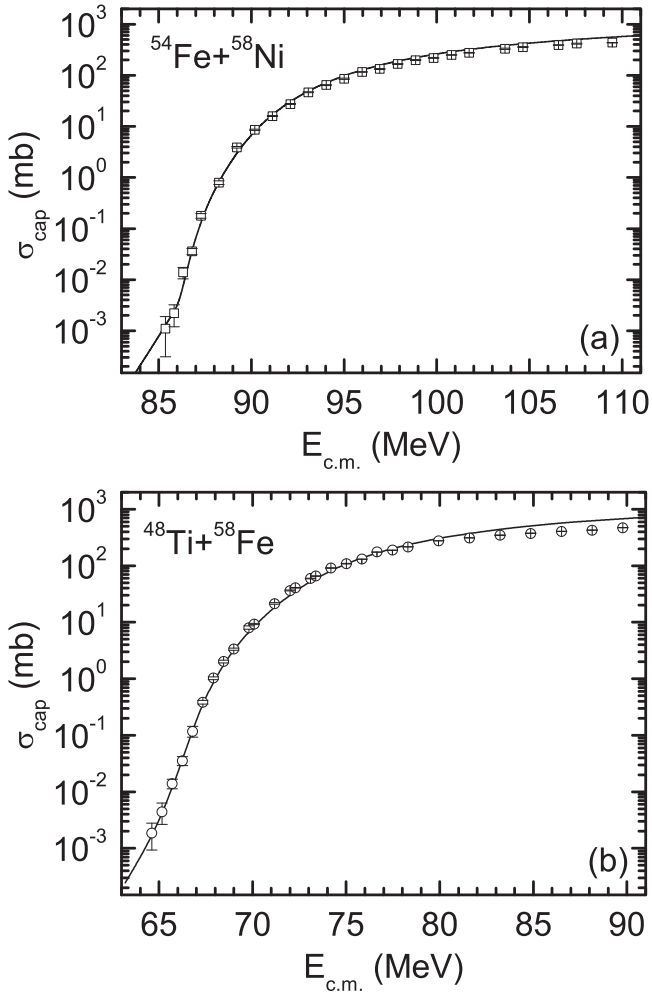

FIG. 4. Calculated fusion (capture) cross sections vs $E_{c.m.}$ (solid lines) for the indicated reactions. The experimental data (symbols) are from Refs. [7,8]. The experimental data have uncertainty bars because of the uncertainties of experimental $\sigma_{cap}(E_{c.m.})$ and $E_{c.m.}$.

As a result, the transfer suppresses the capture process at sub-barrier energies. Thus, the relative enhancement of the sub-barrier fusion cross sections in the ^{48}Ti + ^{58}Fe reaction with respect to those in the ^{58}Ni + ^{54}Fe reaction is not related to the transfer effect. The observed fusion enhancement arises due to the larger deformation of ^{56,58}Fe with respect to one of ^{54}Fe, i.e., the observed effect is purely the deformation effect.

Note that in the reactions ^{58}Ni + ^{54}Fe and ^{48}Ti + ^{58}Fe the calculated s-wave capture probabilities are almost equal to unity at $E_{c.m.} > V_b + 8$ MeV (Fig. 2). It is not clear why the extracted s-wave capture probabilities at this energy range are considerably smaller than unity (about 2 times). The additional experimental and theoretical studies of the normalizations of the capture probabilities and, correspondingly, the cross sections are necessary.

C. *S* factors

At energies below the Coulomb barrier, where the cross section drops rapidly with decreasing energy, it is more convenient to discuss the astrophysical S factor,

$$S(E_{c.m.}) = E_{c.m.}\sigma_{fus}(E_{c.m.})\exp[2\pi(\eta - \eta_0)], \quad (8)$$

rather than the fusion excitation function. Here, $\eta(E_{c.m.}) = Z_1 Z_2 e^2\sqrt{\mu/(2\hbar^2 E_{c.m.})}$ is the Sommerfeld parameter [^{58}Ni + ^{54}Fe($\eta_0 = 63.55$) and ^{48}Ti + ^{58}Fe($\eta_0 = 54.57$)], $\eta_0 = \eta(E_{c.m.} = V_b)$, and Z_1 and Z_2 are the charge numbers of projectile and target nuclei, respectively. The Gamow factor $\exp[-2\pi\eta]$ accounts for some part of the strong energy dependence of the fusion cross section. The S factor is often employed to extrapolate the measured cross section to low energy in the astrophysical reactions. For the medium-heavy systems with $Z_1 Z_2[A_1 A_2/(A_1 + A_2)]^{1/2} > 1500$, the Q value for the complete fusion is negative. This means that the fusion cross section and, correspondingly, S factor must vanish at deep sub-barrier energies, $E_{c.m.} < -Q$. On the other hand, the S factor increases with decreasing energy above and near the Coulomb barrier. Therefore, the S factor must have a maximum. At energies below the Coulomb barrier, the experimental S factor exhibits a clear maximum in some reactions, which is taken as a signature of the fusion hindrance [6].

Assuming that the capture cross section is equal to the fusion cross section, we calculate the astrophysical S factor presented in Fig. 5. A good agreement of the calculated excitation function with the experimental data leads to a good description of the S factor as well. However, one can see slightly different behaviors of S factors for these two reactions. In the case of the ^{58}Ni + ^{54}Fe reaction, the S factor has a well-pronounced maximum. After this maximum the S factor decreases with decreasing $E_{c.m.}$ and then starts to increase. Note, that a similar behavior has been revealed in Ref. [25] by extracting the S factor from the experimental data for lighter systems. In the quantum diffusion approach the existence of the maximum-minimum in the S factor is related to the change of the regime of interaction (the turning-off the nuclear forces and friction) at sub-barrier energies [9]. As the nuclei ^{58}Ni + ^{54}Fe are almost spherical, this change occurs in a certain narrow interval of sub-barrier energy. In the case of the ^{48}Ti + ^{58}Fe reaction, the maximum of the S factor is not clearly observed. The large deformation of heavy nucleus leads to different turning points depending on the mutual orientation of colliding nuclei (or to a large energy interval where the change of the regime of interaction occurs). As a result, the maximum of the S factor could be slightly expressed or even vanished. However, more experimental data at low energies are needed to confirm our predictions.

D. *L* factors

An alternative indirect representation of the measured cross section uses the so-called L factor, the logarithmic derivative of the energy-weighted cross section, namely,

$$L(E_{c.m.}) = \frac{d\ln[E_{c.m.}\sigma_{cap}(E_{c.m.})]}{dE_{c.m.}}.$$

It is a convenient way of characterizing the steep falloff of the measured cross sections [2,6]. One can obtain the relation

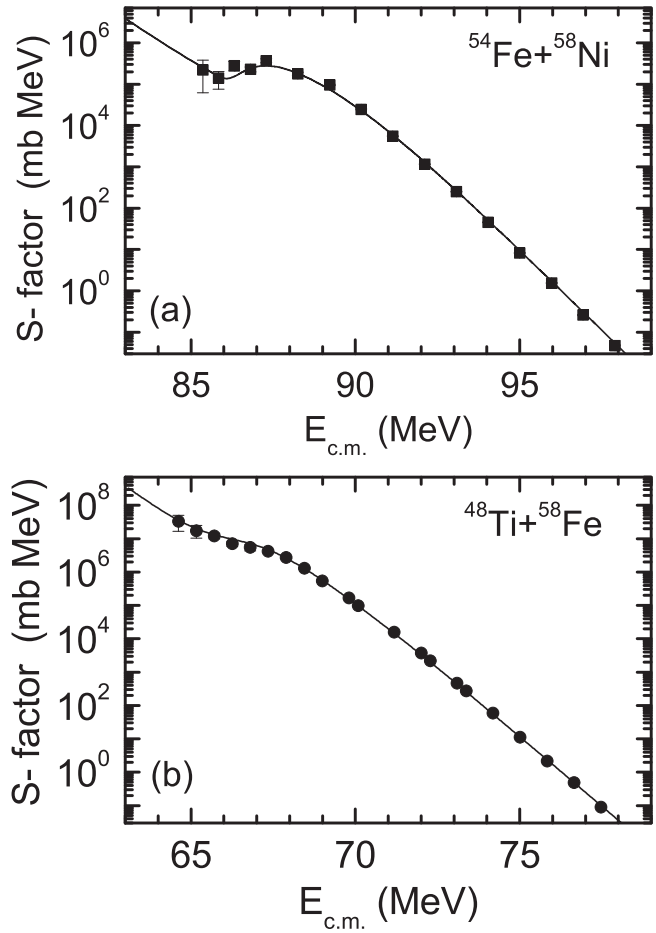

FIG. 5. The calculated (lines) and experimental (symbols [7,8]) astrophysical S factor vs $E_{\mathrm{c.m.}}$ for the indicated reactions. The experimental data have uncertainty bars because of the uncertainties of experimental $\sigma_{\mathrm{fus}}(E_{\mathrm{c.m.}})$ and $E_{\mathrm{c.m.}}$.

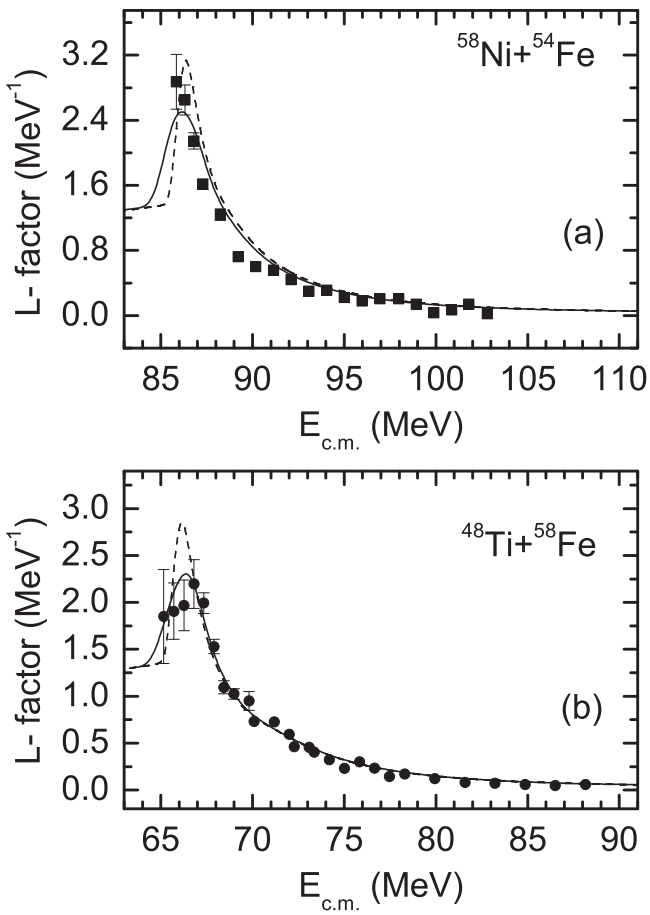

FIG. 6. The calculated (lines) and experimental (symbols [7,8]) logarithmic derivatives of the excitation functions for the indicated reactions. The experimental L factor is obtained as the incremental ratio for successive pairs of experimental energy points of the of the excitation function. In the calculations, $\triangle E_{\mathrm{c.m.}} = 0.4$ MeV (dashed lines) and $\triangle E_{\mathrm{c.m.}} = 0.8$ MeV (solid lines) are used. The experimental data have uncertainty bars because of the uncertainties of experimental $\sigma_{\mathrm{cap}}(E_{\mathrm{c.m.}})$ and $E_{\mathrm{c.m.}}$.

between S factor and L factor:

$$\frac{dS(E_{\mathrm{c.m.}})}{dE_{\mathrm{c.m.}}} = S(E_{\mathrm{c.m.}})[L(E_{\mathrm{c.m.}}) - \pi\eta/E_{\mathrm{c.m.}}].$$

When the S factor reaches a maximum ($\frac{dS}{dE_{\mathrm{c.m.}}} = 0$), the L factor will have reached a value $L = L_{CS} = \pi\eta/E_{\mathrm{c.m.}}$ that exceeds the expectations based on the standard Woods-Saxon–based coupled-channels calculations [2,6]. Note that the s-wave capture probability and L factor are related with each other:

$$L(E_{\mathrm{c.m.}}) = \frac{\pi R_b^2}{E_{\mathrm{c.m.}}\sigma_{\mathrm{cap}}(E_{\mathrm{c.m.}})} P_{\mathrm{cap}}(E_{\mathrm{c.m.}}, J = 0).$$

In Fig. 6, we compare the calculated and the experimental

$$L(E_{\mathrm{c.m.}}) \approx \frac{\ln\left[\left(E_{\mathrm{c.m.}} + \frac{\Delta E_{\mathrm{c.m.}}}{2}\right)\sigma_{\mathrm{cap}}\left(E_{\mathrm{c.m.}} + \frac{\Delta E_{\mathrm{c.m.}}}{2}\right)\right] - \ln\left[\left(E_{\mathrm{c.m.}} - \frac{\Delta E_{\mathrm{c.m.}}}{2}\right)\sigma_{\mathrm{cap}}\left(E_{\mathrm{c.m.}} - \frac{\Delta E_{\mathrm{c.m.}}}{2}\right)\right]}{\Delta E_{\mathrm{c.m.}}}$$

factors. The logarithmic slopes of the excitation functions have a steep rise in the barrier region with decreasing energy. Then, the $L(E_{\mathrm{c.m.}})$ has a very narrow maximum. With the smaller energy increment this maximum becomes more pronounced. The existence of the maximum of experimental $L(E_{\mathrm{c.m.}})$ is clearly seen for the $^{48}\mathrm{Ti} + {}^{58}\mathrm{Fe}$ reaction, while for the $^{58}\mathrm{Ni} + {}^{54}\mathrm{Fe}$ reaction the maximum of $L(E_{\mathrm{c.m.}})$ is not observed. As seen, the experimental points are very close to the region of the maximum. We hope that the further experimental data of fusion cross section at lower energies will confirm our prediction of the maximum of $L(E_{\mathrm{c.m.}})$ for the $^{58}\mathrm{Ni} + {}^{54}\mathrm{Fe}$ reaction at an energy about 6 MeV below the Coulomb barrier. For the systems under consideration, we did not find the fusion hindrance effects and the existence of the maximum

in the L factor is related to the change of the regime of interaction at the sub-barrier energies.

E. Barrier distributions

The barrier distribution is defined as [26]

$$BD(E_{\text{c.m.}}) = d^2[E_{\text{c.m.}}\sigma_{\text{cap}}(E_{\text{c.m.}})]/dE^2_{\text{c.m.}} = \sigma_{\text{cap}}(E_{\text{c.m.}})E_{\text{c.m.}}\left(\frac{dL(E_{\text{c.m.}})}{dE_{\text{c.m.}}} + [L(E_{\text{c.m.}})]^2\right). \quad (9)$$

In Fig. 7, the distributions BD are extracted from the experimental (with $\Delta E_{\text{c.m.}} \approx 1$ MeV [7,8]) and theoretical excitation functions employing a three-point difference approximation [27]

$$BD(E_{\text{c.m.}}) \approx \frac{2E_{\text{c.m.}}\sigma_{\text{cap}}(E_{\text{c.m.}}) - E_{\text{c.m.}}\sigma_{\text{cap}}(E_{\text{c.m.}} + \Delta E_{\text{c.m.}}) - E_{\text{c.m.}}\sigma_{\text{cap}}(E_{\text{c.m.}} - \Delta E_{\text{c.m.}})}{(\Delta E_{\text{c.m.}})^2}. \quad (10)$$

It is clear that with a small energy step $\Delta E_{\text{c.m.}}$ one can approximate the analytical derivative better. However, a large $\Delta E_{\text{c.m.}}$ reduces the experimental uncertainty of BD [27]. In Fig. 7, the calculated BD have one well-pronounced maximum at $E_{\text{c.m.}} = V_b$ as in the experiments [7,8] and perfectly fits the experimental data. It is seen that in the theoretical calculations $V_b = 72.3$ and 91.8 MeV in the reactions ^{48}Ti + ^{58}Fe and ^{58}Ni + ^{54}Fe, respectively. The increase of the deformations of colliding nuclei causes a larger width of barrier distribution. There is no structure at low energies below the main peak of the barrier distribution. At deep sub-barrier energies, the L factor is a more sensitive tool for the excitation function analyses than the BD. The term $[L(E_{\text{c.m.}})]^2$ and the factor $\sigma_{\text{cap}}(E_{\text{c.m.}})E_{\text{c.m.}}$ in Eq. (9) hide any irregularity of the slope in the barrier distribution.

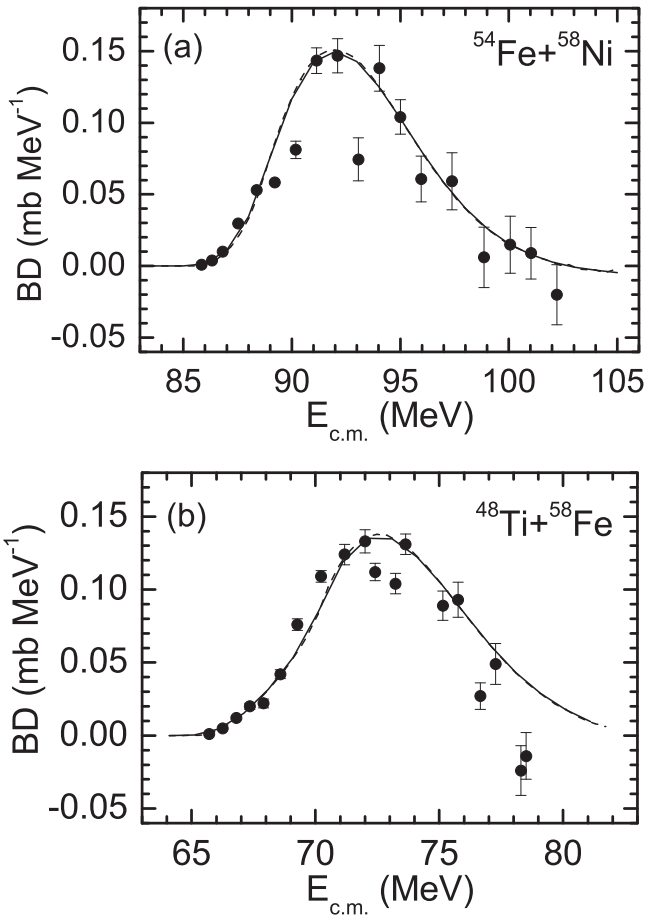

FIG. 7. The calculated (lines) and experimental (symbols [7,8]) fusion barrier distributions BD [Eq. (10)] for the indicated reactions. For the calculated BD, $\Delta E_{\text{c.m.}} = 0.4$ MeV (dashed lines) and $\Delta E_{\text{c.m.}} = 1.0$ MeV (solid lines) are used. For the extraction of the experimental BD, the energy step is $\Delta E_{\text{c.m.}} \approx 1$ MeV. The experimental data have uncertainty bars because of the uncertainties of experimental $\sigma_{\text{cap}}(E_{\text{c.m.}})$ and $E_{\text{c.m.}}$.

Note that the extracted values of BD are very sensitive to the error-bars in σ_{cap} [28]. These error-bars and their dependence on energy perhaps create random deviations of experimental points from the calculated curves at $E_{\text{c.m.}} > V_b$ in Fig. 7. In Ref. [28] it has been shown that the errors are decreased through the use of a larger energy spacing in the high energy range (an optimal energy grid) and the fluctuations of the experimental barrier distribution at energies above the Coulomb barrier are lost.

V. SUMMARY

The quantum diffusion approach, the universal fusion function representation, the extracted capture probabilities from the experimental excitation functions are applied to study the fusion excitation functions in the reactions ^{48}Ti + ^{58}Fe and ^{58}Ni + ^{54}Fe. The experimentally observed sub-barrier fusion enhancement in the ^{48}Ti + ^{58}Fe reaction with respect to the ^{58}Ni + ^{54}Fe reaction is explained by the deformation effect.

With the quantum diffusion approach both reactions are described well. The larger deformation of the ^{48}Ti + ^{58}Fe system washes out the maximum of the S factor, while for the ^{58}Ni + ^{54}Fe system with the smaller deformation the maximum is well pronounced in the experimental data. A good agreement of the calculated and experimental L factors is obtained as well. The existence of a maximum in the L factor is predicted in the ^{58}Ni + ^{54}Fe reaction at energy about 6 MeV below the Coulomb barrier. The existence of the extremal points in the S and L factors is related to the change of the regime of the interaction at sub-barrier energies. The oscillations of BD at energies above the barrier do not exist in our calculations.

ACKNOWLEDGMENTS

We are grateful to A. M. Stefanini for providing us experimental data. This work was partly supported by RFBR (Moscow) and DFG (Bonn). The IN2P3(France)-JINR(Dubna) Cooperation Programme is gratefully acknowledged.

[1] L. F. Canto, P. R. S. Gomes, R. Donangelo, and M. S. Hussein, Phys. Rep. **424**, 1 (2006); L. F. Canto, P. R. S. Gomes, R. Donangelo, J. Lubian, and M. S. Hussein, *ibid.* **596**, 1 (2015), and references therein.

[2] B. B. Back, H. Esbensen, C. L. Jiang, and K. E. Rehm, Rev. Mod. Phys. **86**, 317 (2014), and references therein.

[3] S. Hofmann and G. Münzenberg, Rev. Mod. Phys. **72**, 733 (2000).

[4] Y. T. Oganessian, J. Phys. G **34**, R165 (2007).

[5] G. G. Adamian, N. V. Antonenko, and W. Scheid, Lect. Notes Phys. **848**, 165 (2012).

[6] C. L. Jiang *et al.*, Phys. Rev. Lett. **89**, 052701 (2002); **93**, 012701 (2004); C. L. Jiang, H. Esbensen, B. B. Back, R. V. F. Janssens, and K. E. Rehm, Phys. Rev. C **69**, 014604 (2004).

[7] A. M. Stefanini *et al.*, Phys. Rev. C **92**, 064607 (2015).

[8] A. M. Stefanini *et al.*, Phys. Rev. C **82**, 014614 (2010).

[9] V. V. Sargsyan, G. G. Adamian, N. V. Antonenko, and W. Scheid, Eur. Phys. J. A **45**, 125 (2010).

[10] V. V. Sargsyan, G. G. Adamian, N. V. Antonenko, W. Scheid, and H. Q. Zhang, Phys. Rev. C **84**, 064614 (2011).

[11] V. V. Sargsyan, G. G. Adamian, N. V. Antonenko, W. Scheid, and H. Q. Zhang, Eur. Phys. J. A **47**, 38 (2011); Phys. Rev. C **85**, 024616 (2012); **85**, 037602 (2012); **86**, 014602 (2012); **91**, 014613 (2015); V. V. Sargsyan, G. G. Adamian, N. V. Antonenko, W. Scheid, C. J. Lin, and H. Q. Zhang, *ibid.* **85**, 017603 (2012).

[12] V. V. Sargsyan, G. G. Adamian, N. V. Antonenko, W. Scheid, and H. Q. Zhang, Eur. Phys. J. A **49**, 54 (2013).

[13] R. A. Kuzyakin, V. V. Sargsyan, G. G. Adamian, N. V. Antonenko, E. E. Saperstein, and S. V. Tolokonnikov, Phys. Rev. C **85**, 034612 (2012); V. V. Sargsyan, A. S. Zubov, G. G. Adamian, N. V. Antonenko, and S. Heinz, *ibid.* **88**, 054609 (2013); V. V. Sargsyan, G. Scamps, G. G. Adamian, N. V. Antonenko, and D. Lacroix, *ibid.* **88**, 064601 (2013); V. V. Sargsyan, G. G. Adamian, N. V. Antonenko, and Z. Kohley, *ibid.* **92**, 054613 (2015).

[14] L. R. Gasques, L. C. Chamon, D. Pereira, M. A. G. Alvarez, E. S. Rossi, C. P. Silva, and B. V. Carlson, Phys. Rev. C **69**, 034603 (2004).

[15] L. F. Canto, P. R. S. Gomes, J. Lubian, L. C. Chamon, and E. Crema, J. Phys. G **36**, 015109 (2009).

[16] L. F. Canto, P. R. S. Gomes, J. Lubian, L. C. Chamon, and E. Crema, Nucl. Phys. A **821**, 51 (2009).

[17] C. Y. Wong, Phys. Rev. Lett. **31**, 766 (1973).

[18] A. B. Balantekin, S. E. Koonin, and J. W. Negele, Phys. Rev. C **28**, 1565 (1983); A. B. Balantekin and P. E. Reimer, *ibid.* **33**, 379 (1986); A. B. Balantekin, A. J. DeWeerd, and S. Kuyucak, *ibid.* **54**, 1853 (1996).

[19] V. V. Dodonov and V. I. Man'ko, Trudy Fiz. Inst. AN **167**, 7 (1986).

[20] G. G. Adamian, A. K. Nasirov, N. V. Antonenko, and R. V. Jolos, Phys. Part. Nucl. **25**, 583 (1994).

[21] K. Washiyama, D. Lacroix, and S. Ayik, Phys. Rev. C **79**, 024609 (2009).

[22] R. A. Broglia, C. H. Dasso, S. Landowne, and A. Winther, Phys. Rev. C **27**, 2433 (1983); R. A. Broglia, C. H. Dasso, S. Landowne, and G. Pollarolo, Phys. Lett. B **133**, 34 (1983).

[23] S. Szilner *et al.*, Phys. Rev. C **76**, 024604 (2007); **84**, 014325 (2011).

[24] S. Raman, C. W. Nestor, Jr., and P. Tikkanen, At. Data Nucl. Data Tables **78**, 1 (2001).

[25] K. Langanke and S. E. Koonin, Nucl. Phys. A **410**, 334 (1983); A. Redder *et al.*, *ibid.* **462**, 385 (1987).

[26] N. Rowley, G. R. Satchler, and P. H. Stelson, Phys. Lett. B **254**, 25 (1991).

[27] H. Timmers *et al.*, Nucl. Phys. A **633**, 421 (1998); Phys. Lett. B **399**, 35 (1997).

[28] L. F. Canto and R. Donangelo, Phys. Rev. C **79**, 037601 (2009).